Progress In Electromagnetics Research C, Vol. 76, 171–183, 2017

A Compact Microstrip Lowpass Filter with Sharp Roll-off Rate and Ultra-Wide Stopband Employing Coupled Polygon Patches

Ashkan Abdipour, Arash Abdipour, and Fereshteh Lorestani*

Abstract—In this paper, a microstrip lowpass filter with −3 dB cutoff frequency of 1.8 GHz composed of two resonators with different polygon patches and six symmetric suppressing cells is presented. To design the proposed filter, the impact of each microstrip transmission line on the scattering parameters of the employed resonators is separately determined by extracting the equations of the insertion loss (S_{21}) and return loss (S_{11}) on the basis of their equivalent LC circuit. The designed filter is fabricated and measured, and a good agreement between the results of simulation and measurement is obtained. In the whole stopband region, a return loss better than −0.35 dB and an acceptable suppression level of −22 dB from 1.87 to 19.75 GH are achieved. Furthermore, a flat insertion loss in the passband and an acceptable return loss (−19.32 dB) in this band can verify desired in-band performance. The designed lowpass filter has a high figure of merit about 36969.34.

1. INTRODUCTION

Microstrip lowpass filters (LPFs) are one of the most important components utilized widely in wireless communication systems. Several compact LPFs have been proposed to achieve a desired frequency response such as wide stopband with high rejection level and sharp roll-off. For example, in [1], a microstrip lowpass filter with quasi-elliptic response using both loaded radial-shape patches and meandered main transmission line is proposed. However, it suffers from a gradual transition band and low level of stopband rejection. To expand the stopband region in the frequency response of LPFs, hairpin resonators can be utilized [2–6]. By utilizing this unit in [2], the stopband is expanded. However, the overall circuit size is relatively large, and the skirt performance is not desired. A method to design an LPF with wide stopband is using stepped impedance hairpin resonator with radial stubs, which is done in [3], but this design does not have a sharp roll-off rate. In [4], by employing stepped impedance hairpin units a compact LPF is proposed. However, this filter has a narrow stopband. In [5], another method proposing an LPF based on an application of shunt open-stubs coupled-line in the structure of hairpin unit is introduced. However, this filter suffers from a gradual transition band and also occupies a large area. In [6], defected ground structure (DGS) as a popular method is applied to design an LPF with sharp rejection, but the proposed circuit cannot be utilized on the metal surface. To design an LPF, rat-race directional couplers are used to operate as bandstop transversal filtering sections (TFSs), in [7]. However, by adopting this method the occupied area is significantly large, and also the rejection band is not widened enough. In [8], a quasi-π-slot resonator and open stubs are employed, and an LPF with sharp transition band is proposed, but the circuit size is relatively large. A microstrip LPF by using triangular and radial patch resonators is designed [9], but this filter suffers from gradual transition band. To design an LPF with wide stopband, a cascaded microstrip coupled-line hairpin unit and semi-circle stepped-impedance shunt stubs are used in [10]. In [11], by employing LC resonant structures and transformed radial stubs, an LPF is proposed. However, the occupied areas of both circuits introduced

Received 30 April 2017, Accepted 26 July 2017, Scheduled 9 August 2017
* Corresponding author: Fereshteh Lorestani (Fereshteh.Lorestani@yahoo.com).
The authors are with the Young Researchers and Elite Club, Kermanshah Branch, Islamic Azad University, Kermanshah, Iran.

in [10] and [11] are relatively large. Two other methods to design an LPF with sharp transition band use asymmetric high-low impedance patches and LC tank resonators, which are reported in [12] and [13], respectively. In [15], a lowpass filter using polygon patch resonant cells, T-shaped resonators and two different suppressing cells is designed; however, this filter does not have a sharp transition band. In this paper, a lowpass filter (LPF) with −3 dB cutoff frequency located on 1.8 GHz is proposed. The designed LPF is composed of two main resonators with polygon patches and six suppressing cells to omit the aforementioned defects of the frequency response.

2. FILTER STRUCTURE AND ANALYSIS

2.1. The Primary Resonator Structure and Analysis

The configuration of the primary resonator employing polygon patch and its equivalent LC circuit is illustrated in Fig. 1(a). As illustrated in Fig. 1(b), the transmission lines determined by TL1 in Fig. 1(a) are modeled by L2. The shown capacitance (C1) and inductor (L1) account for the polygon patch and high impedance transmission line determined by TL2, respectively. C2, C3 and C4 model the capacitance between the microstrip structure and the ground. To adjust the −3 dB cutoff frequency of primary resonator around the desired operating frequency of 1.8 GHz, the influences of variables on the frequency response should be determined. Thus, the equations of insertion loss ($S''21$) and return loss ($S''11$) of the primary resonator shown in Fig. 1(a) on the basis of its LC circuit are calculated. The $ABCD$ parameters of a two-port network are given by [15]:

$$A = \frac{V_1}{V_2}|_{I_2=0}, \quad B = \frac{V_1}{-I_2}|_{V_2=0}, \quad C = \frac{I_1}{V_2}|_{I_2=0}, \quad D = \frac{I_1}{-I_2}|_{V_2=0} \tag{1}$$

The $ABCD$ parameters of the primary resonance cell shown in Fig. 1(a) can be given as follows:

$$A = \frac{\omega^2 C_1 L_2}{\omega^2 C_1 L_1 - 1} + 1 \tag{2}$$

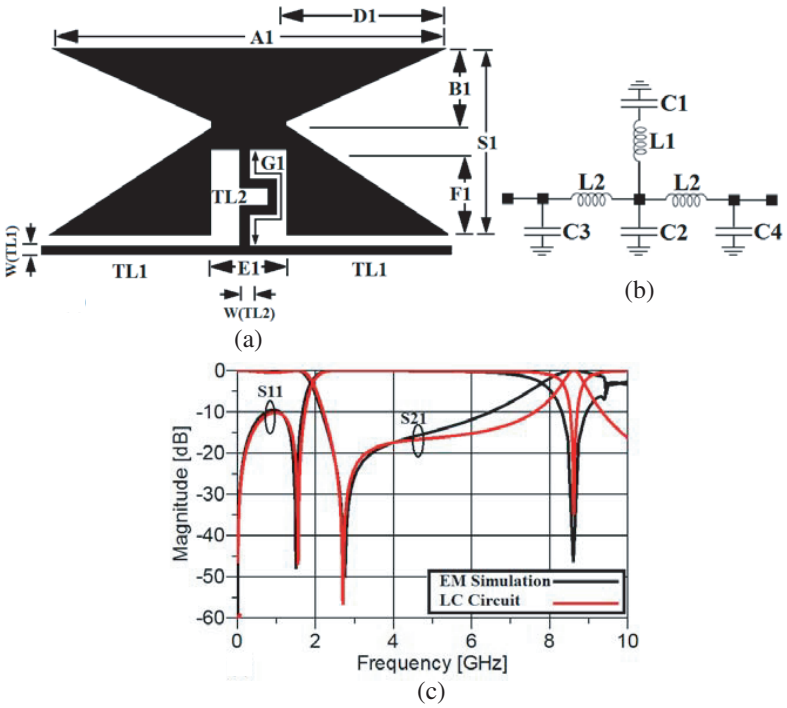

Figure 1. (a) The configuration of the primary resonator with polygon patch. (b) The equivalent LC circuit of the primary resonator. (c) The EM simulation result and the frequency response of LC circuit of the primary structure.

$$B = \frac{j\omega^2 L_2^2 C_1 + 2j\omega^3 L_2 L_1 C_1 - 2j\omega L_2}{1 - \omega^2 C_1 L_1} \tag{3}$$

$$C = \frac{j\omega C_1}{1 - \omega^2 C_1 L_1} \tag{4}$$

$$D = \frac{\omega^2 C_1 L_2}{\omega^2 C_1 L_1 - 1} + 1 \tag{5}$$

According to the obtained ABCD parameters, the equations of insertion loss ($S''21$) and return loss ($S''11$) of the primary resonator are as follows [15]:

$$S''_{11} = \frac{A + \frac{B}{Z_0} - CZ_0 - D}{A + \frac{B}{Z_0} + CZ_0 + D}, \quad S''_{22} = \frac{-A + \frac{B}{Z_0} - CZ_0 + D}{A + \frac{B}{Z_0} + CZ_0 + D} \tag{6}$$

$$S''_{12} = \frac{2(AD - CB)}{A + \frac{B}{Z_0} + CZ_0 + D}, \quad S''_{21} = \frac{2}{A + \frac{B}{Z_0} + CZ_0 + D} \tag{7}$$

As a result, the s-parameters can be obtained as follows

$$S''_{11} = S''_{22} = \frac{j\omega^3 L_2 C_1 (L_2 + 2L_1) - j\omega L_2 (L_2 + C_1)}{2Z_0 (1 - \omega^2 C_1 L_2 - \omega^2 C_1 L_1) + j\omega^3 L_2 C_1 (1 + 2L_1) - j\omega L_2 (L_2 + C_1)} \tag{8}$$

$$S''_{12} = S''_{21} = \frac{2Z_0 \left(1 - \omega^2 C_1 L_1\right)}{2Z_0 (1 - \omega^2 C_1 L_2 - \omega^2 C_1 L_1) + j\omega^3 L_2 C_1 (1 + 2L_1) - j\omega L_2 (L_2 + C_1)} \tag{9}$$

According to Eqs. (8) and (9), the insertion loss and return loss can be controlled by changing the values of L1 and C1. As it mentioned, the polygon patch and transmission line determined by TL2 are modeled by the capacitor and inductor, respectively. Therefore, to clarify their effects on the frequency response,

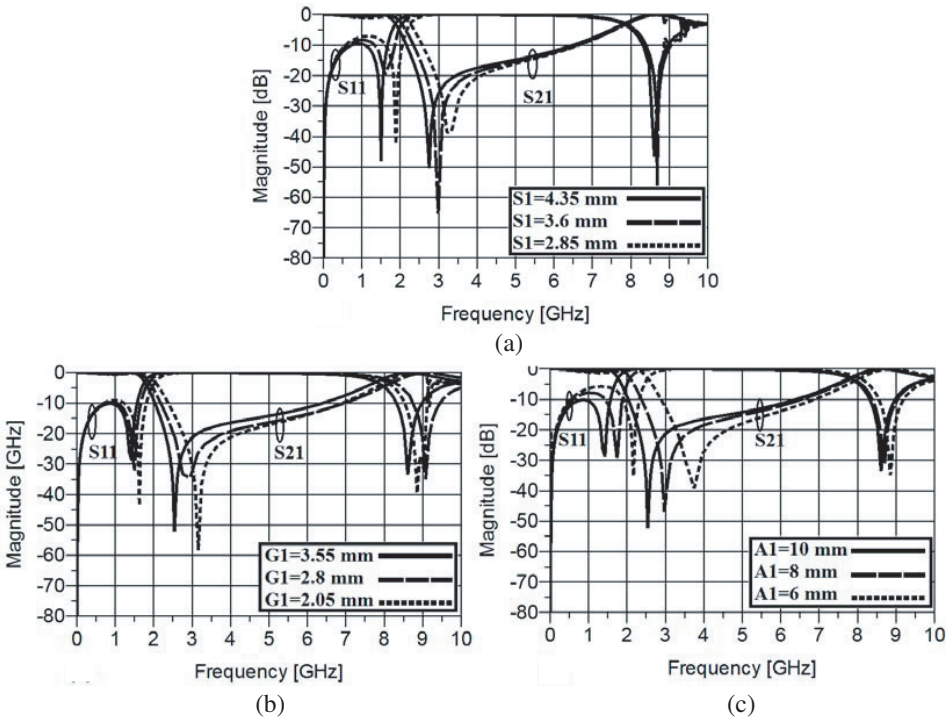

Figure 2. The behavior of the main resonator against changing the values of S1, G1 and A1.

their corresponding microstrip realizations can be used, instead. In order to display how changing the dimensions of the mentioned corresponding microstrip lines can affect the frequency response, several full-wave simulations versus A1, S1 and G1 are plotted in Figs. 2(a), (b) and (c), respectively. As can be observed from Fig. 2, by increasing the values of all three variables, the transition zero will move to lower frequencies causing a sharper transition band. Furthermore, these increases lead to decreasing the return loss level in the pass band region. Note that by changing the values of S1, from 2.85 to 4.25 mm with steps of 0.75, and also the value of A1 from 6 to 10 mm with steps of 2, the −3 dB cutoff frequency will move toward lower frequencies, significantly.

The dimensions of the shown resonator in Fig. 1(a) are: $A1 = 10$ mm, $B1 = 1.75$ mm, $D1 = 3.8$ mm, $E1 = 2.1$ mm, $F1 = 2.25$ mm, $G1 = 3.55$ mm, $S1 = 4.35$ mm, $W(TL1) = W(TL2) = 0.1$ mm. The values of lumped elements of the shown equivalent LC in Fig. 2(b) are [15]: $L1 = 2.884$ nH, $C1 = 1.21$ pF, $L2 = 6.01$ nH, $C2 = 0.248$ pF and $C3 = C4 = 0.14$ pF. Note that the values of inductors and capacitances are obtained based on RO4003 substrate with a thickness of 0.508 mm and permittivity of 3.38. The EM simulation and frequency response of LC circuit of the primary resonator are illustrated in Fig. 1(c), which are in good agreement. According to the shown frequency response of the primary resonator in Fig. 1(c), the return loss and insertion loss in the passband are better than 0.49 and 9.5 dB, respectively. Furthermore, the primary resonance cell creates a transition zero at 2.755 GHz with an attenuation level of −50.411 dB bringing about a suppressing band of −10.4 dB from 2.17 to 6.458 GHz. As observed, the primary resonator does not have acceptable stopband characteristics and suffers from gradual skirt performance.

2.2. The Main Resonator Structure and Analysis

The configuration of the main resonator employing two primary resonators which are placed symmetrically around (X) axis and its equivalent LC circuit are illustrated in Figs. 3(a) and (b), respectively.

Similar to the primary resonator, to find which variables can affect the frequency response and

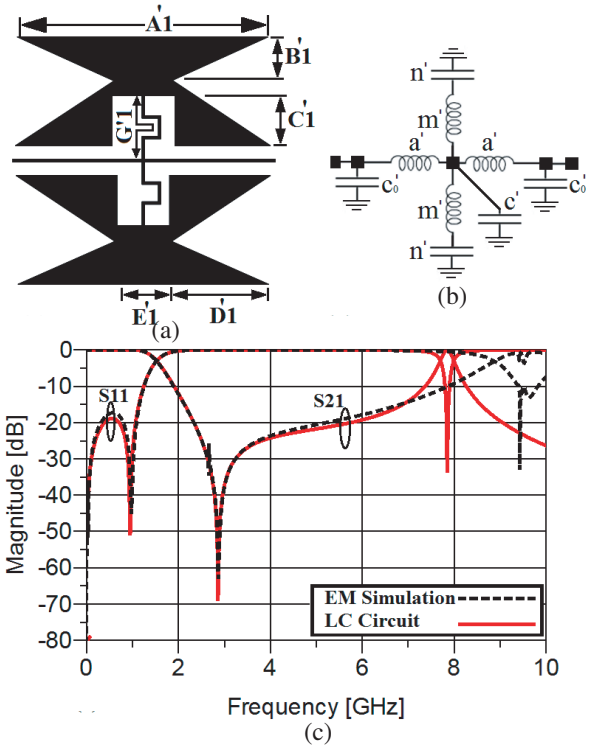

Figure 3. (a) The configuration of the first main resonator with two polygon patches. (b) Its equivalent LC circuit. (c) The EM simulation result and the frequency response of LC circuit of the main structure.

in particular the location of the transmission zero, the equations of insertion loss ($S'21$) and return loss ($S'11$) of the first main resonator shown in Fig. 3(a) on the basis of its equivalent LC circuit are obtained as follows:

$$S'_{11} = \frac{\left(2a'x's + y'a'^2s^2 - y'Z_0^2\right)}{\left(2Z_0x' + 2Z_0a'y's + 2a'x's + y'a'^2s^2 + y'Z_0^2\right)} \tag{10}$$

$$S'_{21} = \frac{\left(2Z_0x'\right)}{\left(2Z_0x' + 2Z_0a'y's + 2a'x's + y'a'^2s^2 + y'Z_0^2\right)} \tag{11}$$

where

$$x' = \left(1 + m'n's^2\right) \tag{12}$$

$$y' = \left[\left(1 + m'n'c's^2\right) + \left(c' + 2n'\right)s\right] \tag{13}$$

Clearly the location of the TZ can be adjusted by changing the values of m' and n'. In order to depict how the values of their corresponding microstrip realizations can affect the frequency response, several full-wave simulations versus A'1, B'1 and G'1 are plotted in Figs. 4(a), (b) and (c), respectively. In this case, the remaining parameters in Fig. 3(a) are kept constant.

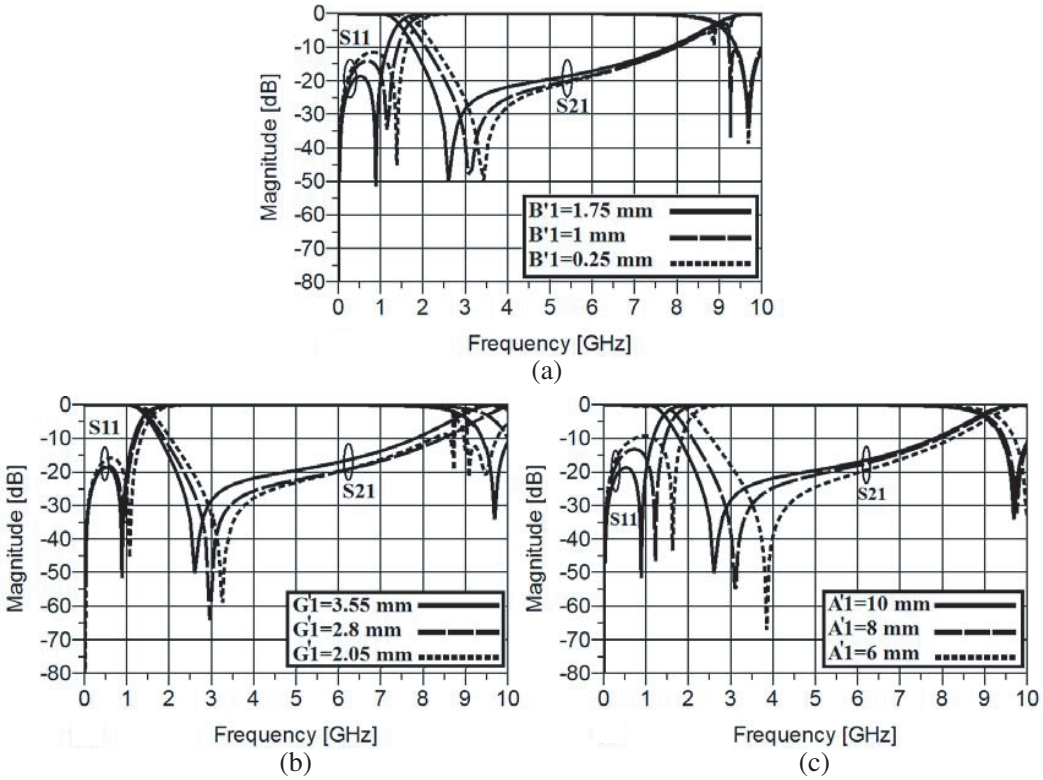

Figure 4. The behavior of the main resonator against changing the values of B'1, G'1 and A'1.

As can be seen from Fig. 4(a), by increasing the value of B'1 from 0.25 to 1.75 mm with steps of 0.75 and also the value of A'1 from 6 to 10 mm with steps of 2, the transition zero at 3.438 GHz will move to lower frequencies causing a sharper cutoff and better return loss level in the passband. Moreover, the -3 dB cutoff frequency will move toward lower frequencies. As shown in Fig. 4(b), decreasing the value of G'1 from 2.05 to 3.55 mm with steps of 0.75, the transmission zero at 3.22 GHz will shift to lower frequencies making the roll-off rate sharper. Finally, the main resonator with -3 dB cutoff frequency of 1.667 GHz is designed. According to the depicted EM simulation result in Fig. 3(c), the stopband of the main resonator can suppress a frequency range from 2.23 up to 7.14 GHz with a suppressing level

of -15 dB. Moreover, this resonator creates a transition zero (TZ) at 2.913 GHz with corresponding attenuation level of -62.978 dB creating a gradual roll-off rate (45.6 dB/GHz). The dimensions of the illustrated resonator in Fig. 3(a) are: $A'1 = 10.09$ mm, $B'1 = 1.8$ mm, $D'1 = 3.83$ mm, $E'1 = 2.16$ mm, $F'1 = 2.28$ mm, $G'1 = 3.55$ mm, $S1 = 4.35$ mm. The values of lumped elements of the shown equivalent LC in Fig. 3(b) are [15]: $C'0 = 0.1$ pF, $C' = 0.6$ pF, $a' = 1.405$ nH, $n' = 0.52$ pF, $m' = 2.595$ nH.

2.3. The Second Main Resonator Structure and Analysis

The configuration of the second main resonator composed of four high-low impedance resonators with polygon patches which are placed symmetrically around (y) axis and its equivalent LC circuit are illustrated in Figs. 5(a) and (b), respectively.

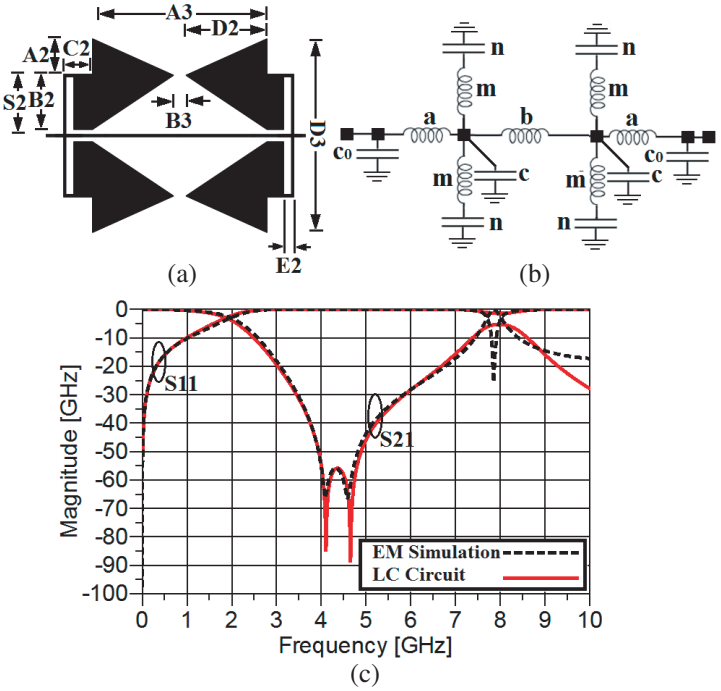

Figure 5. (a) The configuration of the second main resonator. (b) The lumped circuit of the second resonator. (c) The EM simulation and the frequency response of the lumped circuit of the second resonator.

Similar to the first resonator, the role of each section on controlling the frequency response is determined by extracting the equations of the insertion loss (S_{21}) and return loss (S_{11}) of the second resonator according to its LC circuits as follows:

$$S_{11} = \frac{\left(4Z_O^2 x^2 B'^2 A' + A'B'^4 - A'^3 B'^2\right)}{(B'^5 - A'^2 B'^3)} \tag{14}$$

$$S_{21} = \frac{8Z_O^3 x^3 B'^2}{1 - A'^2 B'^2} \tag{15}$$

where

$$A' = 2axs + ya^2 s^2 - yZ_O^2 \tag{16}$$

$$B' = 2axs + ya^2 s^2 + 2Z_O x + 2Z_O ays + yZ_O^2 \tag{17}$$

$$x = \left(1 + mns^2\right) \tag{18}$$

$$y = \left[\left(1 + mncs^3\right) + (c + 2n)\, s\right] \tag{19}$$

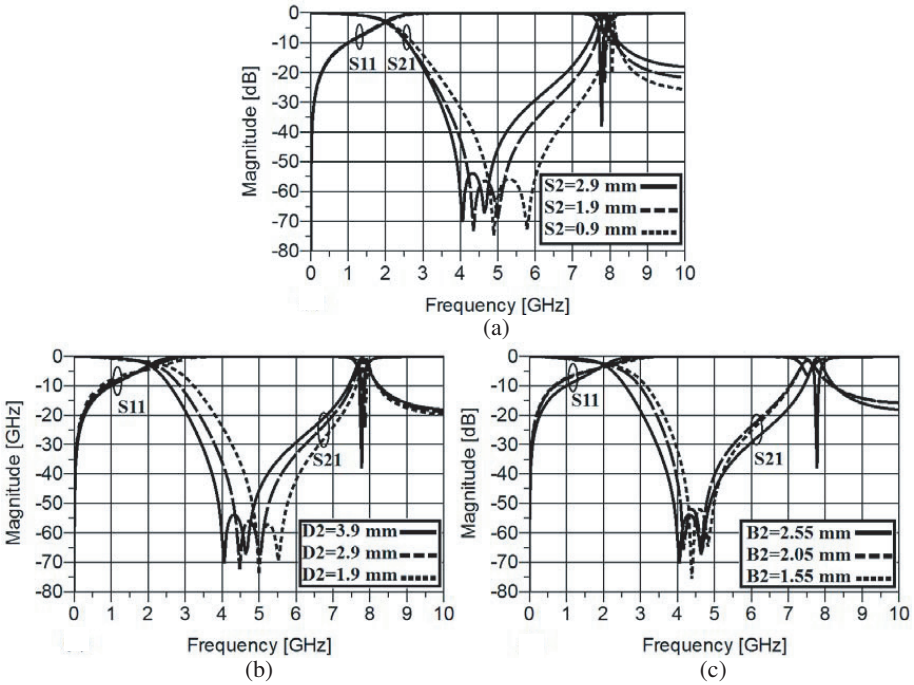

Figure 6. The behavior of the main resonator against changing the values of: (a) S2, (b) D2 and (c) B2

According to Equations (14)–(19), the frequency response of the shown resonator in Fig. 5(a) can be controlled by changing the capacitances and inductances values. For instance, according to the calculated insertion loss and return loss, (m) and (n) play vital roles in the performance of the mentioned resonator. To clarify the impact of changing (m) and (n) on the frequency response, their corresponding microstrip realizations can be considered instead. Therefore, several full-wave simulations versus S2, D2 and B2 are plotted in Fig. 6. Figs. 6(a) and (b) illustrate the behavior of the designed resonator against changing the value of S2 and D2. By increasing the values of the S2 and D2 from 0.9 to 2.9 mm with steps of 1 and from 1.9 to 3.9 mm with steps of 1, respectively, the transition zero at around 4.8 GHz will move to lower frequencies causing a sharper transition band. However, these increases do not affect the return loss in the passband region. The frequency response of the second resonator against changing the value of B2 is shown in Fig. 6(c). As observed, by enhancing the value of B2 with steps of 0.5, the -3 dB operating frequency will approach lower frequencies. Moreover, this increase not only sharpens the transition band but also improves the return loss level in the passband. Eventually, a resonator with acceptable frequency response employing four resonance cells with polygon patches is obtained. The dimensions of the resonator illustrated in Fig. 5(a) are: $A2 = 1.7$ mm, $B2 = 2.65$ mm, $C2 = 1.4$ mm, $D2 = 3.9$ mm, $E2 = 0.1$ mm, $S2 = 2.95$ mm, $A3 = 10.4$ mm, $B3 = 2.6$ mm, $D3 = 9.3$ mm. The values of inductors and capacitors of the shown equivalent LC in Fig. 5(b) are: $C0 = 0.1$ pF, $C = 0.609$ pF, $a = 1.872$ nH, $b = 3.744$ nH, $n = 0.51$ pF, $m = 2.595$ nH. The EM simulation and frequency response of lumped circuit of the second resonator operating at 1.98 GHz are depicted in Fig. 5(c), which are in good agreement. According to the illustrated frequency response of this resonator, the insertion loss in the passband is approximately zero from DC up to 1.208 GHz. Furthermore, the mentioned resonance cell creates a pair of transition zeros at 4.063 GHz and 4.635 GHz (TZ2) with attenuation levels of -64.421 and -64.457 dB, respectively, bringing about a suppressing band with attenuation level of -20 dB from 3 GHz to 6.638 GHz.

2.4. The Effects of Mutual Coupling between the Two Primary Resonators

The combination of the two main resonators, its equivalent LC circuit and their frequency responses are shown in Figs. 7(a), (b) and (c). Clearly, the combination of the first and second main resonators

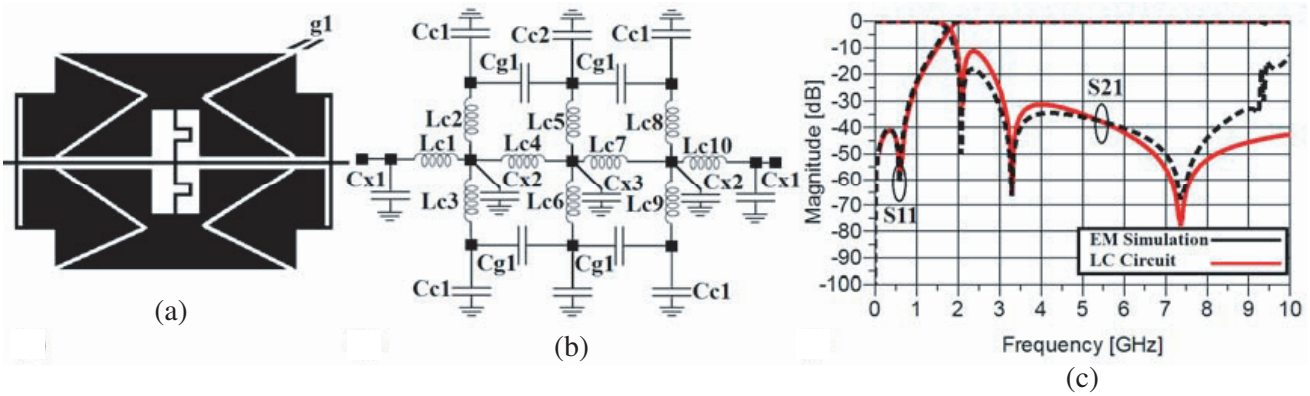

Figure 7. (a) The combination of the first and second main resonators. (b) Its lumped circuit. (c) The EM simulation and the frequency response of the lumped circuit of the combined resonator.

leads to creating a gap determined by g1 in Fig. 7(a). This gap is modeled by Cg1 in the equivalent LC circuit, as shown in Fig. 7(b).

The values of inductors and capacitors of the shown equivalent LC in Fig. 7(b) are: $Lc1 = 0.225\,\text{nH}$, $Lc2 = 2.595\,\text{nH}$, $Lc3 = 2.595\,\text{nH}$, $Lc4 = 1.85\,\text{nH}$, $Lc5 = 4.54\,\text{nH}$, $Lc6 = 4.54\,\text{nH}$, $Lc7 = 1.85\,\text{nH}$, $Lc8 = 2.595\,\text{nH}$, $Lc9 = 2.595\,\text{nH}$, $Lc10 = 0.225\,\text{nH}$, $Cg1 = 70\,\text{fF}$, $Cc1 = 0.635\,\text{pF}$, $Cc2 = 0.58\,\text{pF}$, $Cx1 = 1.5\,\text{fF}$, $Cx2 = 35\,\text{fF}$, $Cx3 = 63.5\,\text{fF}$. To clarify the effects of the above-mentioned gap on the frequency response particularly, several simulations versus changing value of Cg1 are plotted in Fig. 8. As can be seen, by increasing the value of Cg1 from 0 to 140 fF with steps of 70, the operating frequency and the first transmission zero at 2.5 GHz with corresponding attenuation level of 40.195 dB will move to lower frequencies, but these increases do not affect the other two transmission zeros located on higher frequencies significantly. Moreover, the attenuation level of the first transmission zero decreases leading to lower level of suppression in the stopband around this zero. Note that changing the value of Cg1 does not influence the return loss.

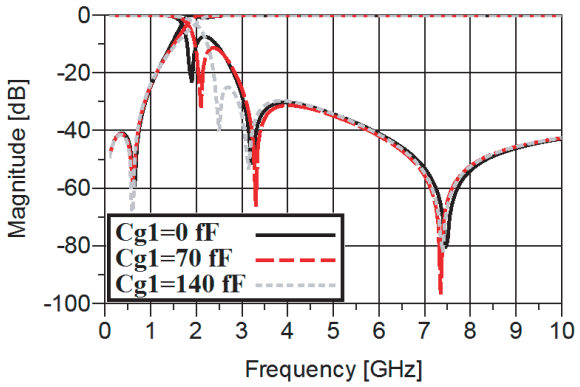

Figure 8. The behavior of the combination of the first and second main resonators against changing value of Cg1.

2.5. The Employed Suppressing Cells Structure and the Final Filter Design

In the next stage, to widen the rejection band, there is a need for suppressing cells. Utilizing these rejecting units leads to creating some transmission nulls, thus transmission peaks will be suppressed, and consequently the stopband region will be expanded.

Two conventional suppression units to extend the stopband are high-low impedance resonators with rectangular patches and open-stubs.

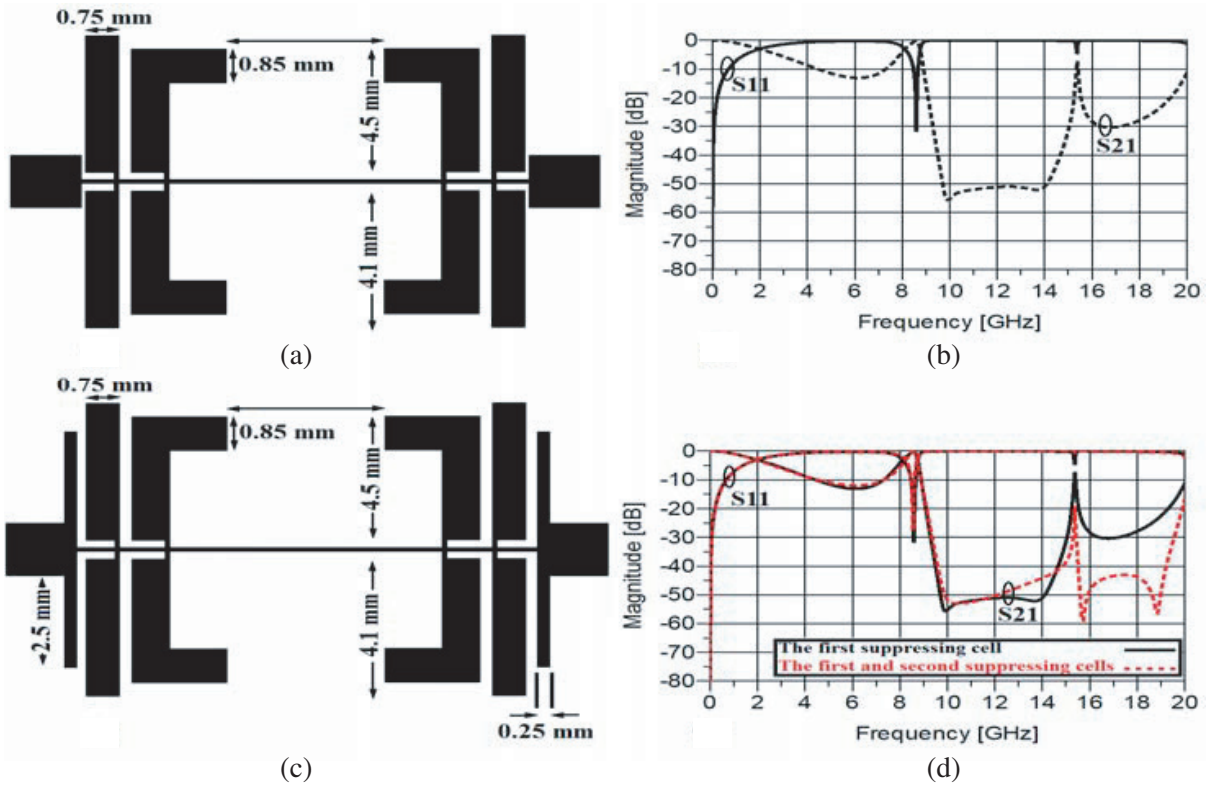

Figure 9. (a) The schematic of the first suppressing cell. (b) The frequency response of the first suppressing cell. (c) The schematic of the first and second suppressing cells. (d) The frequency response of the first and second suppressing cells.

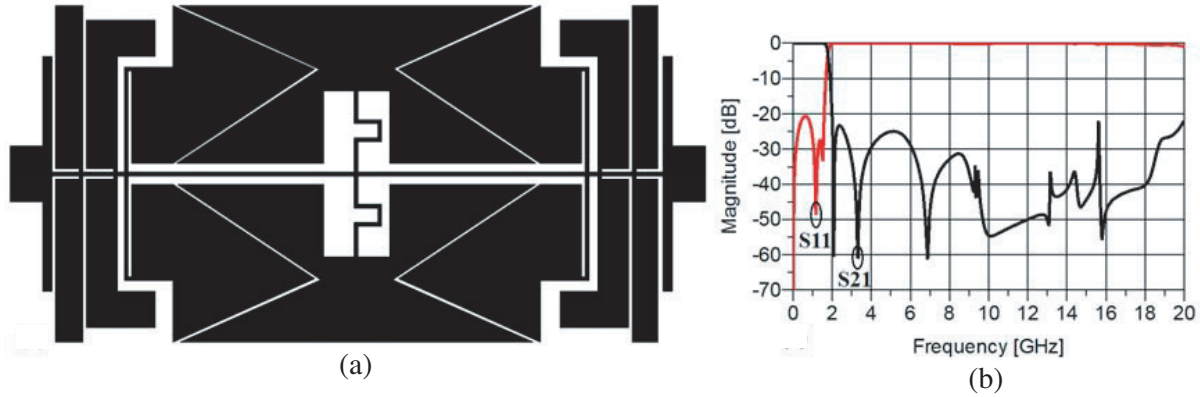

Figure 10. (a) The configuration of the proposed LPF. (b) The frequency response of the proposed LPF.

Figures 9(a) and (b) show the schematic and frequency response of a pair of high-low impedance resonators with different dimensions as the first suppressing cells, which create three transmission zeros at 9.995, 13.75 and 16.94 GHz with corresponding attenuation levels of −55.402, −52.162 and −30.19 dB, respectively. Clearly, this cell is not capable of rejecting spurious frequencies from 18.1 to 20 GHz. Thus, there is a need for using another suppressing resonator capable of suppressing spurious frequencies in the mentioned range. Fig. 9(c) shows two open-stubs which are added to the first rejecting cells creating an effective transmission zero at 18.87 GHz (TZs3) with corresponding attenuation level of −56.387 dB (see Fig. 9(d)). This can help the first suppressing cell suppress spurious frequencies in a wider range.

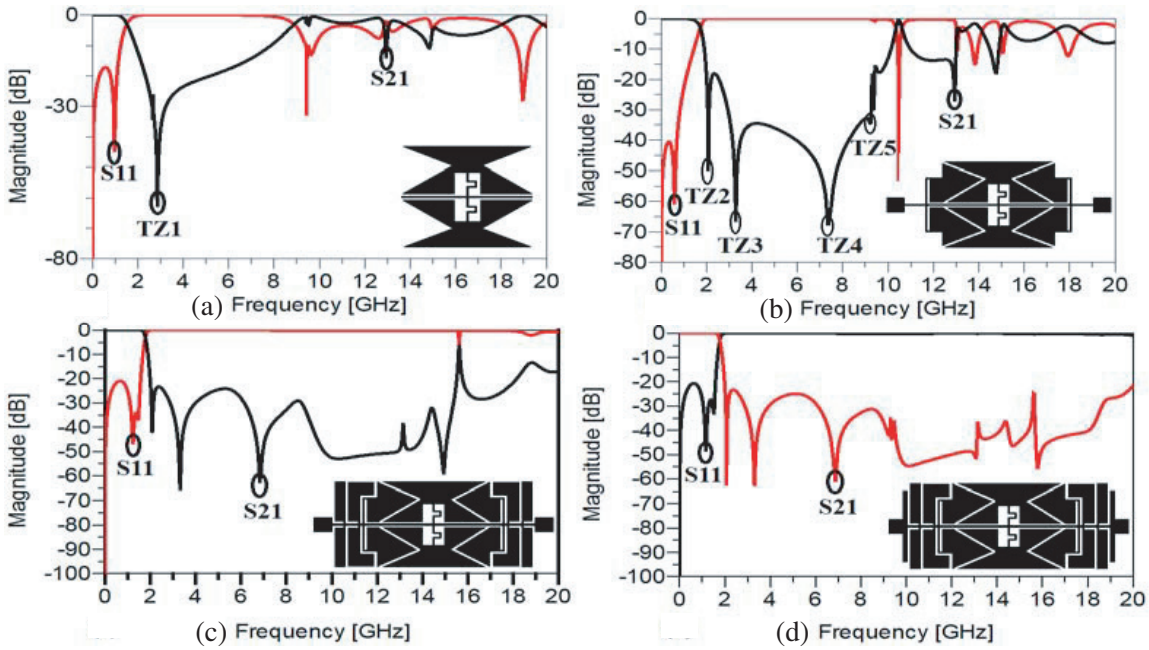

Figure 11. The frequency response of (a) resonator 1, (b) resonators 1 and 2, (c) resonators 1, 2 and the first suppressing cell, (d) resonators 1, 2, and both suppressing cells.

Finally, the introduced resonators and suppressing cells are combined leading to obtaining a lowpass filter with sharp roll-off and ultra-wide stopband at 1.8 GHz, as illustrated in Fig. 10. The procedures of combining the employed resonators and the impact of adding each resonator on the frequency response are depicted in Fig. 11, step by step. As observed from Fig. 11(a), the first resonator has a −3 dB cutoff frequency at 1.667 GHz and a transmission zero (TZ1) at 2.913 GHz with attenuation level of −62.978 dB. Moreover, in this resonator a stopband from 2.23 up to 7.14 GHz with corresponding attenuation level better than −15 dB is obtained. However, resonator 1 does not have a sharp roll-off and wide stopband bandwidth. In order to improve the skirt performance, four resonance cells with different polygon patches as second main resonator are added, as illustrated in Fig. 11(b). The combination of resonators 1 and 2 has four transmission zeros (TZ2, TZ3, TZ4 and TZ5) at 2.083, 3.295, 7.361 and 9.226 GHz with corresponding attenuation levels of −50.059, 66.756, −34.591 and −67.954 dB, respectively. In fact, by adding resonator 2 the transition zero of resonator 1, TZ1, is shifted to the lower frequencies, and TZ2 is obtained. Shifting TZ1 to lower frequencies leads to a sharp transition band about 0.318 GHz from −3 to −40 dB. Furthermore, the second resonators create two new transition zeros of TZ3 and TZ4. However, the stopband bandwidth is not desired. To widen the stopband with a high suppressing level, eight high-low impedance resonators as the first suppressing cells can be employed, as shown in Fig. 11(c). By combining resonators 1, 2 and the first suppressing cells, the stopband can reject spurious frequencies from 1.921 up to 15.48 GHz and also from 15.86 up to 17.98 GHz with a suppressing level better than −22.8 dB. Furthermore, the insertion loss less than −0.05 dB and return loss better than −20 dB in the passband are obtained

In order to expand the stopband bandwidth more than 10 fc ($fc = 1.8$ GHz) with an attenuation level of −22 dB, the second suppressing cells, i.e., two open-stubs, are employed. Finally, a compact LPF with −3 dB cutoff frequency of 1.8 GHz, a sharp transition band (208.8 dB/GHz) and an ultra-wide stopband (17.986 GHz) is designed, as shown in Fig. 11(d).

3. MEASUREMENT AND SIMULATION RESULTS

A photograph of the proposed LPF is illustrated in Fig. 12(a). The proposed LPF is designed, fabricated and tested.

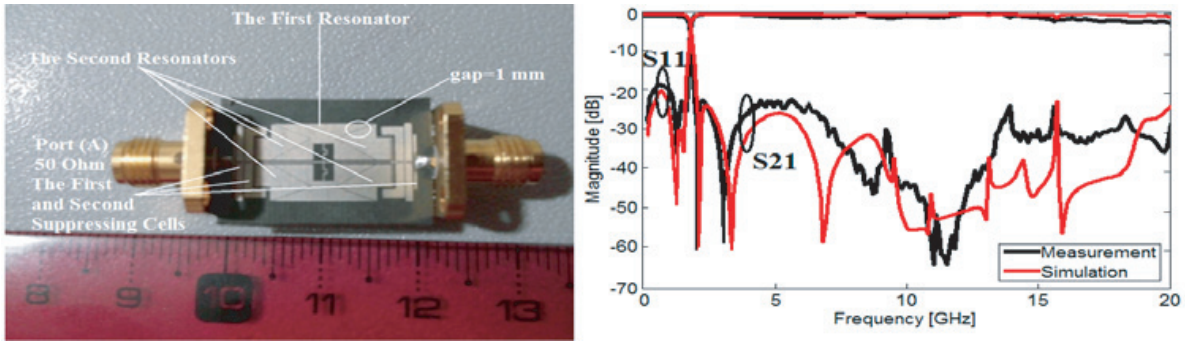

Figure 12. (a) The configuration of the proposed LPF. (b) The results of simulation and measurement of the proposed LPF.

The implemented LPF is constructed on an RO4003 substrate with a thickness of 0.508 mm and permittivity of 3.38. The simulation and measurement results of the designed LPF are carried out by using an EM-simulator ADS based on the method of moments and a HP8757A network analyzer, respectively. The simulation and measurement frequency responses of the proposed LPF are illustrated in Fig. 12(b). As can be seen, −3 dB cutoff frequency of the filter is located on 1.8 GHz. According to the measurement results, in the whole passband region the insertion loss is close to zero, and also in this band, the return loss is better than −19.32 dB. As observed, close to the operating frequency two transmission zeros with attenuation levels of −60.386 and −58.747 exist causing a sharp cutoff. Thanks to these TZs, an acceptable roll-off rate equal to 206.51 (dB/GHz) is measured. The stopband region suppresses spurious frequencies from 1.87 to 19.75 GHz with corresponding rejection level of −22 dB. Moreover, in the rejection band a flat return loss better than −0.35 dB is obtained. The circuit size of the proposed filter is about 18.1×9.3. Table 1 shows the performance comparison of the other published works and the proposed LPF. In this table, the roll-off rate is defined as:

$$\zeta = \frac{\alpha_{\max} - \alpha_{\min}}{f_s - f_c} \text{ (dB/GHz)} \tag{20}$$

where $\alpha_{\max}$ is the −40 dB attenuation point, $\alpha_{\min}$ the −3 dB attenuation point, f_s the −40 dB stopband

Table 1. Comparison between the performance of the proposed Lowpass Filter and previous works.

Ref.	RO (ζ)	RSB	SF	NCS	AF	FOM
[1]	36.3	1.323	1.5	0.079×0.079	1	11543
[2]	37	1.15	2	0.280×0.076	1	3999
[3]	30	1.25	1.5	0.0800×0.080	1	8789
[4]	74	1.19	2	0.114×0.105	1	14713
[5]	95	1.4		0.214×0.104	1	11951
[6]	130	0.933	2	0.227×0.089	2	6004
[7]	200	1.36	2	0.801×0.374	1	1815.9
[8]	82	1.28	2.5	0.110×0.220	1	10842
[9]	37	1.65	1.5	0.111×0.091	1	9065
[10]	61.6	1.44	1	0.272×0.236	1	1386
[11]	62	1.72	3	0.310×0.240	1	4430
[14]	185	1.666	2.1	0.227×0.177	1	16181
This Work	**206.51**	**1.66**	**2.2**	$\mathbf{0.200 \times 0.102}$	1	**36969.34**

frequency, and f_c the -3 dB cutoff frequency. The relative stopband bandwidth (RSB) is given by:

$$\text{RSB} = \frac{\text{stopband bandwidth}}{\text{stopband center frequency}} \tag{21}$$

The relative stopband bandwidth (RSB) of the lowpass filter is about 166%. The suppression factor (SF) is based on the stopband suppression. For example, if the stopband suppression is under 22 dB, then the SF is considered as 2.2. The normalized circuit size (NCS) is given by:

$$\text{NCS} = \frac{\text{physical size (length} \times \text{width)}}{\lambda g^2} \tag{22}$$

where λ_g is the guided wavelength at 3 dB cutoff frequency. The architecture factor (AF) can be recognized as the complexity factor of the circuit, which is defined as 1 when the design is 2D and as 2 when the design is 3D. Finally, the figure-of-merit (FOM) is the overall index of the proposed filter, which is defined as:

$$\text{FOM} = \frac{RSB \times \zeta \times \text{SF}}{\text{AF} \times \text{NCS}} \tag{23}$$

4. CONCLUSION

In this paper, a microstrip lowpass filter with -3 dB cutoff frequency at 1.8 GHz composed of two resonators with different triangular patches and four suppressing cells is proposed. To design the presented filter, the influence of each microstrip transmission line on the scattering parameters of the utilized resonators is determined by calculating the equations of the insertion loss (S_{21}) and return loss (S_{11}) based on their equivalent LC circuits, respectively. Next, by combining the two main resonators with different coupled triangular patches, a sharp transition band is obtained. Then, to achieve a high relative stopband bandwidth four high-low impedance resonators as suppressing cells are utilized. Furthermore, on the basis of the measurement and simulation results which are in good agreement, a flat insertion loss in the passband and a low return loss in the stopband verify the desired in-band and out-band frequency response.

REFERENCES

1. Wang, J., L. J. Xu, S. Zhao, Y. X. Guo, and W. Wu, "Compact quasi-elliptic microstriplowpass filter with wide stopband, "*IEE Electron. Lett.*, Vol. 46, No. 20, 1384–1385, 2010.
2. Luo, S., L. Zhu, and S. Sun, "Stopband-expanded low-pass filters using microstrip coupled-line hairpin units," *IEEE Microw. Wireless Compon. Lett.*, Vol. 18, No. 8, 506–508, Aug. 2008.
3. Wei, X. B., P. Wang, M. Q. Liu, and Y. Shi, "Compact wide-stopband lowpass filter using stepped impedance hairpin resonator with radial stubs," *IEE Electron. Lett.*, Vol. 47, No. 15, 862–863, Jul. 2011.
4. Li, L., Z. F. Li, and J. F. Mao, "Compact lowpass filters with sharpand expanded stopband using stepped impedance hairpin units," *IEEE Microw. Wireless Compon. Lett.*, Vol. 20, No. 6, 31–312, Jun. 2010.
5. Velidi, V. K. and S. Sanyal, "Sharp roll-off lowpass filter with wide stopband using stub-loaded coupled-line hairpin unit," *IEEE Microw. Wireless Compon. Lett.*, Vol. 21, No. 6, 30–303, Jun. 2011.
6. Mandal, M. K., P. Mondal, S. Sanyal, and A. Chakrabarty, "Low insertion-loss, sharp rejection and compact microstriplowpass filter," *IEEE Microw. Wirel. Compon. Lett.*, Vol. 16, No. 11, 600–602, 2006.
7. Gomez-Garcia, R., M. A. Sanchez-Soriano, M. Sanchez Renedo, G. Torregrosa-Penalva, and E. Bronchalo, "Extended-stopband microstrip lowpass filter using rat-race directional coupler," *Electron. Lett.*, Vol. 49, No. 4, 272–274, 2013.
8. Wang, C. J. and C. H. Lin, "Compact lowpass filter with sharp transition knee by utilizing a quasi-π-slot resonator and open stubs," *IET Microw. Antennas Propag.*, Vol. 4, No. 4, 512–517, 2010.

9. Wang, J., H. Cui, and G. Zhang, "Design of compact microstrip lowpass filter with ultra-wide stopband," *IEE Electron. Lett.*, Vol. 48, No. 14, 854–856, Jul. 2012.
10. Wei, F., L. Chen, X.-W. Shi, Q.-L. Huang, and X.-H. Wang, "Compact lowpass filter with wide stop-band using coupled-line hairpin unit," *Electron. Lett.*, Vol. 46, No. 1, 88–90, 2010.
11. Ma, K. and K. S. Yeo, "New ultra-wide stopband low-pass filter using transformed radial stubs," *IEEE Trans. Microw. Theory. Tech.*, Vol. 59, No. 3, 604–611, Mar. 2011.
12. Abdipour, A., Ar. Abdipour, and S. Lotfi, "A lowpass filter with sharp roll-off and high relative stopband bandwidth using asymmetric high-low impedance patches," *Radioengineering*, Vol. 24, No. 3, 712–716, 2015.
13. Nouritabar, A. R., A. Abdipour, and Ar. Abdipour, "A design of low-pass filter with wide stopband and sharp roll-off rate using series LC tanks resonator," *Applied Computational Electromagnetics Society (ACES) Journal*, Vol. 31, No. 11, 1343–1350, 2016.
14. Abdipour, Ar. and A. Abdipour, "Compact microstrip lowpass filter with an ultra-wide stopband and sharp transition band using T-shaped and polygon resonators," *Progress In Electromagnetics Research C*, Vol. 74, 51–61, 2017.
15. Hong, J.-S. and M. J. Lancaster, *Microstrip Filters for RF/Microwave Applications*, John Wiley & Sons, Inc., 2001.